

## Multiresolution Isogeometric Topology Optimisation Using Moving Morphable Voids

Bingxiao Du<sup>1</sup>, Yong Zhao<sup>1,\*</sup>, Wen Yao<sup>2</sup>, Xuan Wang<sup>3</sup> and Senlin Huo<sup>1</sup>

**Abstract:** A general and new explicit isogeometric topology optimisation approach with moving morphable voids (MMV) is proposed. In this approach, a novel multiresolution scheme with two distinct discretisation levels is developed to obtain high-resolution designs with a relatively low computational cost. Ersatz material model based on Greville abscissae collocation scheme is utilised to represent both the Young's modulus of the material and the density field. Two benchmark examples are tested to illustrate the effectiveness of the proposed method. Numerical results show that high-resolution designs can be obtained with relatively low computational cost, and the optimisation can be significantly improved without introducing additional DOFs.

**Keywords:** Isogeometric analysis (IGA), multiresolution, moving morphable voids (MMV), topology optimisation.

### 1 Introduction

Topology optimisation (TOP) is a powerful tool aiming at finding the best layout of material in a prescribed design domain. Compared with the only size or shape optimisation, TOP can provide a conceptual design for a product without a priori assumption of structural configuration and connectivity, and often achieve better performance. Density-based TOP approaches, such as the homogenization method [Bendsoe and Kikuchi (1988)], SIMP method [Bendsøe and Sigmund (2004)], ESO/BESO method [Huang and Xie (2007)], has been successfully applied to various structural design problems [Wang, Arabnejad, Tanzer et al. (2018)]. The topology in Density-based TOP approaches is represented by the material distribution via discretised cells with reasonable resolution. When utilising these methods, some vital numerical issues have gained much concern, such as grey transition regions and mesh dependency. In order to overcome these issues, nodal based implicit schemes are proposed. The most representative approaches are projection method [Guest, Prévost and Belytschko (2004)] and level set method (LSM) [Wang, Wang and Guo (2003); Allaire, Jouve and Toader (2004)]. Parameterised level set method [Wei, Li, Li et al.

---

<sup>1</sup> College of Aerospace Science and Engineering, National University of Defense Technology, Changsha, 410073, China.

<sup>2</sup> National Innovation Institute of Defense Technology, Chinese Academy of Military Science, Beijing, 100000, China.

<sup>3</sup> School of Civil Engineering, Hefei University of Technology, Hefei, 230009, China.

\*Corresponding Author: Yong Zhao. Email: zhaoyong@nudt.edu.cn.

Received: 19 October 2019; Accepted: 19 November 2019.

(2018); Liu, Li, Wei et al. (2018)] is also popular in TOP community since it could tackle re-initialisation and avoid solving the Hamilton-Jacobi equation. Heaviside projection and level set function are employed to generate crisp and smooth structural boundaries.

However, both the density-based method and the implicit method are not consistent with modern computer-aided-design (CAD) modelling systems. To tackle this problem, Guo et al. [Guo, Zhang and Zhong (2014)] developed a kind of Lagrangian approaches named Moving Morphable Components (MMC) method [Zhang, Zhang and Guo (2016)], which adopt a number of structural components with explicit geometry descriptions as fundamental building blocks of optimisation. Since complex topological shapes and boundaries are rigorously represented by parameterised geometries [Van Miegroet and Duysinx (2007)] and Boolean operations [Burla and Kumar (2008)], it could reduce problem dependency and the computational burden [Dunning (2017)], and allow for a relative high flexibility [Deng and Chen (2016)], deformability [Bujny, Aulig, Olhofer et al. (2017)] and smooth boundaries. This idea has also been investigated to realize the size, shape and topology optimisation together for truss structures [Wei, Ma and Wang (2014)]. Besides, Norato and his colleagues also developed a similar explicit topology optimisation method, which is called the geometric projection method [Norato, Bell and Tortorelli (2015); Zhang, Norato, Gain et al. (2016)]. MMC method has gained much attention in most recent years, and interested readers could refer to Du et al. [Du and Zhu (2019); Zhang, Li, Zhang et al. (2016); Wang, Long, Hoang et al. (2018)] for the application of MMC in various design problems.

As the dual method of MMC, the Moving Morphable Voids (MMV) [Zhang, Yang, Zhou et al. (2017)] method is also proposed to do topology optimisation. The structure boundaries in MMV method are parameterised with closed B-spline curves (CBS) [Zhang, Zhao, Gao et al. (2017)], and the topology change can also be implemented through boundary variation and void insert/merge. MMV has been successfully applied in additive manufacturing-oriented design [Liu, Du, Zhang et al. (2017)], boundary dependent problem [Zhou, Zhang and Zhu (2019)] and geometrically nonlinear problem [Xue, Liu, Zhang et al. (2019)]. When the explicit description is utilised, both MMC and MMV are capable of describing the geometry clearly with a small number of design variables.

Since the topology description model is fully decoupled with the FEA model, special attention should be paid to take advantage of the explicit boundaries. Actually, several effective schemes have been proposed to handle clear boundaries and cut elements. The most representative approaches are Finite Cell Method and the extended Finite Element Methods [Wei, Wang and Xing (2010)]. They have been utilised in the boundary sensitive scenarios like the stress problems [Zhang, Li, Zhou et al. (2018)]. Both of the two methods rely on the partition of sub-elements and adaptive integration to identify the discontinuity inside the cut elements. Recently, the multi-resolution scheme [Nguyen, Paulino, Song et al. (2010)] has also been introduced to the MMC-based approach to get high-resolution optimisation results with sufficient small size geometry features. The basic idea behind this is to use the independent functional spaces for structural analysis and the description of material distribution. Following this idea, Wang et al. [Wang, Kang and He (2013)] and He et al. [He, Kang and Wang (2014)] have successfully improved the computational accuracy and the geometrical description quality of design

boundaries with adaptive refinement, the geometrically nonlinear topology optimisation is also achieved with meshless analysis.

IGA is a computational approach proposed by Hughes et al. [Hughes, Cottrell and Bazilevs (2005)]. The aim of IGA is to employ the same basis functions (e.g., NURBS) to bridge the gap between FEA and computer-aided design (CAD) [Cottrell, Hughes and Bazilevs (2009)]. Comparing with FEA, IGA is capable of eliminating geometry errors from mesh discretisation and solving problems that require high-order derivative of variables. Besides, it requires much fewer DOFs for an analysis.

As an ideal alternative for FEM, IGA has received great attention from researchers in the field of shape optimisation [Wang, Abdalla and Turteltaub (2017); Wang, Turteltaub and Abdalla (2017)] and topology optimisation [Wang, Wang, Xia et al. (2018)]. For density-based methods, Kumar et al. [Kumar and Parthasarathy (2011)] and Qian et al. [Qian (2013)] used high-order B-spline basis functions to form the density of FEM elements. Hassani et al. [Hassani, Khanzadi and Tavakkoli (2012)] employed NURBS to approximate the density field. Dedè et al. [Dedè, Borden and Hughes (2012)] combined IGA with a phase-field model. Liu et al. [Liu, Yang, Hao et al. (2018)] utilised the isogeometric topology optimisation (ITO) to solve stress constrained problems. Gao et al. [Gao, Gao, Luo et al. (2019)] enhanced the smoothness and continuity with Shepard function and high-order NURBS basis functions. To accelerate the computation, Wang et al. [Wang, Liao, Ye et al. (2020)] proposed a high-efficiency ITO scheme, which takes full use of three methods: multilevel mesh, MGCG, and local-update strategy. Regarding LSM, Wang first carried out ITO under LSM scheme [Wang and Benson (2016a, 2016b)]. Lately, the GPU parallel strategy was also introduced to accelerate the optimisation [Xia, Wang, Wang et al. (2017)]. Different optimisation problems [Ghasemi, Park and Rabczuk (2017); Jahangiry and Tavakkoli (2017)] were also considered with LSM-ITO approach. IGA has also been successfully combined with MMC [Hou, Gai, Zhu et al. (2017); Xie, Wang, Xu et al. (2018)]. Moreover, the aforementioned MTO scheme also shows its merits when applied to IGA [Lieu and Lee (2017b)]. The IGA-MTO scheme also shows effectiveness in optimising multi-material structures [Lieu and Lee (2017a)] and spatially graded hierarchical structures [Xu, Wang and Xie (2019)]. Although IGA-MTO shows excellent performance, it has only been applied in density-based methods. An extension with ersatz material model needs to be made to use multiresolution IGA in the explicit topology optimisation scheme.

In this work, a general and new explicit isogeometric MMV optimisation (IGA-TOP-MMV) method is proposed, where the ersatz material model and Greville abscissae collocation scheme are utilised to combine IGA with MMV-TOP. To ensure the optimisation can be significantly improved without fine analysis mesh, a multiresolution optimisation scheme is suggested under the proposed explicit isogeometric MMV framework. Thus, topological geometry with explicit boundaries can be identified by high-resolution material mesh. Benefitting from this scheme, we can obtain high-resolution designs with a relatively low computational cost.

The remainder of this paper is organized as follows: Section 2 gives a brief introduction to the MMV-based TO with CBS, NURBS basis and a general formulation of ITO-MMV. Section 3 presents the IGA-MTO-MMV based design framework and its

combination with the ersatz material model. Sections 4 provides two benchmark cases. Finally, Section 5 draws a conclusion.

## 2 Theoretical basis

### 2.1 MMV-based TO

As described in Guo et al. [Guo, Zhang and Zhong (2014); Zhang, Zhang and Guo (2016)], unlike the traditional topology optimisation method where continuous structures are represented by element densities (in SIMP and evolutionary structural optimisation approach) or nodal values of a level set function, the geometry components or voids based method was recently developed to solving the topology optimisation in an explicit and geometrical way. For the two-dimensional structures in MMV method, the voids are formulated with a set of parametrised closed curves  $C_i$  ( $i=1, \dots, n_v$ ). They are allowed to move, deform, overlap and merge in the design domain freely. Optimised structural topology is obtained by changing the positions and evolving the boundaries of these voids.

#### 2.1.1 Geometric description of moving morphable voids

Here the parameterised topology description function (TDF) is used to describe the shape and topology of moving morphable void. For example, the TDF  $T_i$  of the  $i$ -th void can be expressed as

$$\begin{cases} T_i(\mathbf{x}) < 0, & \text{if } x \in \Omega_i, \\ T_i(\mathbf{x}) = 0, & \text{if } x \in \partial\Omega_i, \\ T_i(\mathbf{x}) > 0, & \text{if } x \in D \setminus \Omega_i, \end{cases} \quad (1)$$

where  $D$  denotes the fixed design domain,  $\Omega$  and  $\partial\Omega$  are the sub-domain occupied by the embedded hole and its boundary.

For a design domain involving  $n$  voids, the TDF of the whole structure can be expressed according to the Boolean operations of all the voids:

$$T = \min(T_1, T_2, \dots, T_n) \quad (2)$$

$$\begin{cases} T(\mathbf{x}) < 0, & \text{if } x \in \Omega^v, \\ T(\mathbf{x}) = 0, & \text{if } x \in \partial\Omega^v, \\ T(\mathbf{x}) > 0, & \text{if } x \in D \setminus \Omega^v \end{cases} \quad (3)$$

where  $\Omega^v = \bigcup_{k=1}^n \Omega_k$  represents the region occupied by voids. This means that, if a point  $x$

lies inside one of MMVs, then the corresponding value of TDF will be less than zero. If a point  $x$  is located at the boundary of one of MMVs, then the corresponding value of TDF will be equal to zero. If a point  $x$  is outside MMVs, then the corresponding value of TDF will be greater than zero.

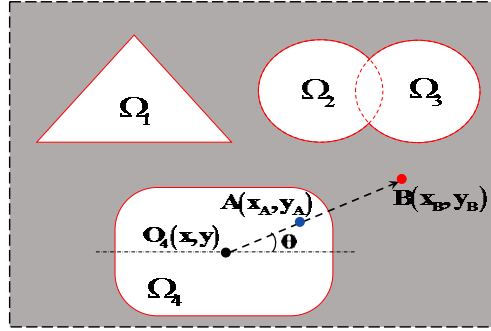


**Figure 1:** Topology defined by moving morphable voids

In this work, the closed B-spline (CBS) curve is adopted to parameterise the boundary of voids. A CBS defined in the polar form can be defined as

$$C_i(\theta) = \sum_{j=1}^n B_{j,p}(\theta) r_j^i \quad (4)$$

$i$  is the index of the CBS,  $j$  is the index of a knot of the CBS.  $r_j^i$  is the distance parameter for the control points  $j$  in the  $i$ -th CBS, which is also considered as the design variable of the optimisation. Control points are restricted along the equally spaced radial direction with respect to the central point  $(x_i, y_i)$ .  $\theta$  in polar coordinate is computed in Cartesian coordinate by

$$\theta_i = \begin{cases} \arctan \frac{y - y_i}{x - x_i}, & x \geq x_i, y \geq y_i \\ \arctan \frac{y - y_i}{x - x_i} + 2\pi, & x \geq x_i, y < y_i \\ \arctan \frac{y - y_i}{x - x_i} + \pi, & x < x_i \end{cases} \quad (5)$$

The corresponding B-spline basis functions  $B_{j,p}$  of degree  $p$  in Eq. (4) are defined with the recursive averaging formula [Piegl and Tiller (2013)]:

$$B_j^0(\theta) = \begin{cases} 1 & \text{if } \theta_j \leq \theta \leq \theta_{j+1} \\ 0 & \text{otherwise} \end{cases} \quad (6)$$

$$B_j^p(\theta) = \frac{\theta - \theta_j}{\theta_{j+p} - \theta_j} B_j^{p-1}(\theta) + \frac{\theta_{j+p+1} - \theta}{\theta_{j+p+1} - \theta_{j+1}} B_{j+1}^{p-1}(\theta)$$

Thus, the parameterised TDF of arbitrary point  $(x, y)$  for the  $i$ -th void can be expressed as

$$T_i(x, y) = C_i^{penal}(\theta(x, y)) - D_i^{penal}(x, y) \quad (7)$$

where  $D_i = \sqrt{(x - x_i)^2 + (y - y_i)^2}$ .  $penal$  is a penalty parameter, which is set to be  $penal = 1$  in our implementation. For example, the centre of the void  $\Omega_4$  is  $O_4$ , the regularised signed

distance of point A and B are  $T_4(x_A, y_A) < 0$  and  $T_4(x_B, y_B) > 0$ , as shown in Fig. 1.

In order to guarantee the smoothness and unified continuity of the closed curve, the periodic closed B-spline curves (PCBS), also named unclamped closed B-spline curves [Yoely, Amir and Hannel (2018)], are suggested [Du, Yao, Zhao et al. (2019)].

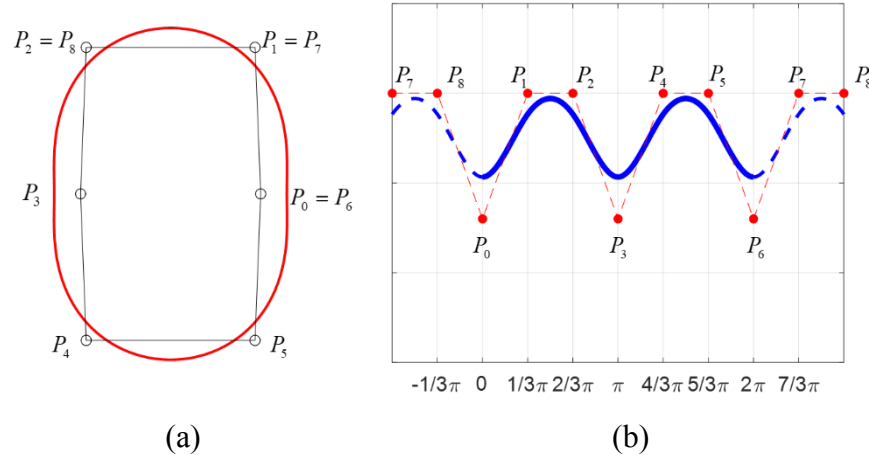


**Figure 2:** Illustration of Cubic PCBS with Control points  $P_i$

Fig. 3 shows the difference between the clamped CBS and unclamped PCBS. The knot vectors in PCBS are periodically repeated before and after the original knot span, then periodic behaviour can be achieved through the repeat of the basis function. Thus, the periodic B-spline satisfy the following condition:

$$B_i^p(\xi) = B_{i+n}^p(\xi) \tag{8}$$

For illustration purpose, Fig. 2, shows a mapping relation of a cubic PCBS from Cartesian coordinate  $\theta Or$  to  $xOy$ , where the figure on the left is the cubic PCBS in the Cartesian coordinate system  $xOy$ , the figure on the right is the cubic PCBS in the Cartesian coordinate system  $\theta Or$ . By differentiating Eq. (7) with respect to distance design variable  $d_j$ , the derivative of  $T_i$  with respect to  $r_j$  gives

$$\frac{\partial T_i}{\partial d_j} = q C_i^{q-1} \frac{\partial C_i}{\partial d_j} = q C_i^{q-1} B_j^p(\theta) \tag{9}$$

Since  $q = 1$  is adopted,  $\frac{\partial T_i}{\partial d_j} = B_j^p(\theta)$ .

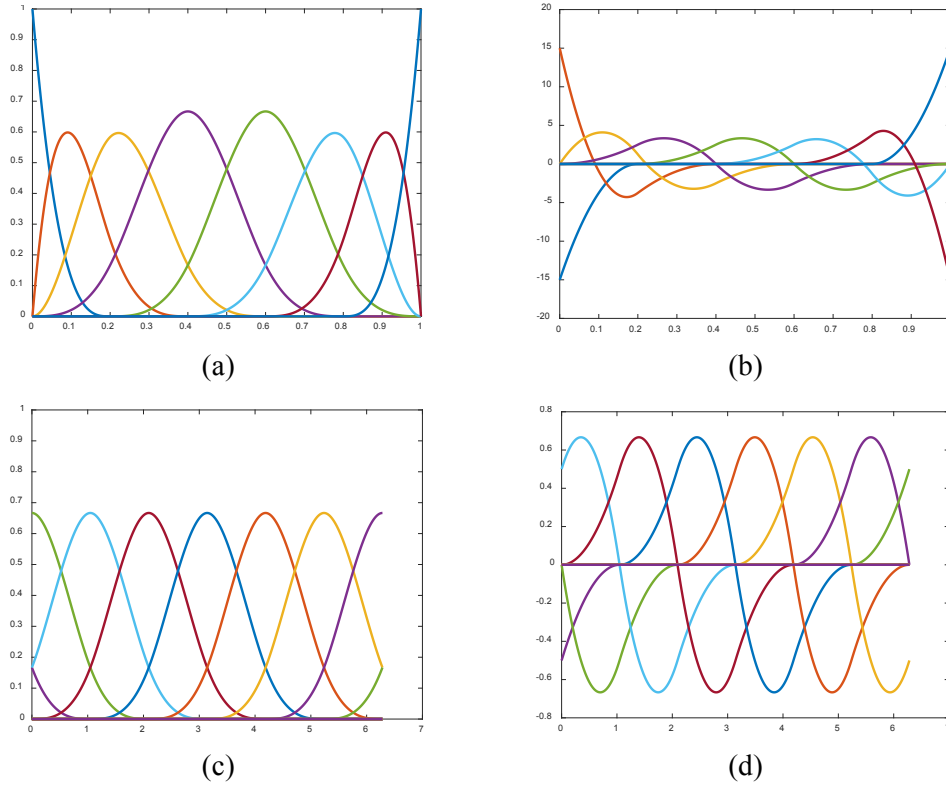


**Figure 3:** Univariate basis functions and their derivatives for clamped and unclamped B-spline

2.1.2 Problem formulation based on MMV

Generally, the topology optimisation problem under MMV-based solution framework can be stated as follows:

$$\begin{aligned}
 &\text{Find } \mathbf{Z} = (\mathbf{Z}^1, \dots, \mathbf{Z}^{nv})^T \\
 &\text{Minimize } Obj = Obj(\mathbf{Z}) \\
 &s.t. \tag{10} \\
 &\quad g_j(\mathbf{Z}) \leq 0, \quad j = 1, \dots, M, \\
 &\quad \mathbf{Z} \subset U_{\mathbf{Z}}
 \end{aligned}$$

where  $\mathbf{Z}^i = \{x^i, y^i, r_1^i, \dots, r_n^i\}$ ,  $i = 1, \dots, nv$  is the vector of design variables describing the TDF of the  $i$ -th PCBS void,  $x^i, y^i$  are the coordinates of void centre,  $r_j^i$  is the distance parameter of the void.  $Obj(\mathbf{Z})$  is the objective function which evaluates the structural performance,  $U_{\mathbf{Z}}$  is the admissible set of the design vector  $\mathbf{Z}$ .  $g_j$  are the constraint functions.

To ensure the optimisation problem can be solved by using gradient-based optimisation algorithms like the method of moving asymptotes (MMA) [Svanberg (1987)], the minimum Boolean operation in Eq. (2) needs to be smoothly approximated by an envelope function like KS function [Li, Li, Gao et al. (2015)], R function [Xie, Wang, Xu et al. (2018)] and p-norm [Zhang, Zhou and Zhu (2017)]. In the present work, the following well-known KS function is used. Thus, the minimum of  $T$  in Eq. (2) can be approximated with  $\tilde{T}$ :

$$\tilde{T} = -\frac{1}{k} \ln \left( \sum_{j=1}^{nv} \left( e^{k(-T_j)} \right) \right) \quad (11)$$

where  $k$  is the control number, set to be 40 in this work.  $nv$  is number of voids as stated in Eq. (10).

## 2.2 IGA for structural analysis

Here we use NURBS-based IGA for structural analysis. In IGA, the given geometry and the unknown solution space are represented by the same NURBS basis functions.

This concise introduction starts from the well-known Cox-de Boor recursion formula described in Eq. (6). To keep consistency with conventional denotation in IGA, we use the parametric coordinates  $\xi$  and  $\eta$  instead of polar coordinates  $\theta$  in Eq. (6). By introducing a positive weight  $w_i$  to each B-spline basis function, a NURBS basis function is defined as

$$N_i^p(\xi) = \frac{w_i B_i^p(\xi)}{\sum_{j=1}^n w_j B_j^p(\xi)} \quad (12)$$

By employing the tensor product of univariate basis functions  $B_i^p(\xi)$  and  $B_j^q(\eta)$  in two parametric dimensions  $\xi$  and  $\eta$  corresponding to two knot vectors  $\Xi = \{\xi_1, \xi_2, \dots, \xi_{n+p+1}\}$  and  $H = \{\eta_1, \eta_2, \dots, \eta_{m+q+1}\}$ , the bivariate B-spline basis functions  $B_{i,j}^{p,q}(\xi, \eta)$  can be expressed as

$$B_{i,j}^{p,q}(\xi, \eta) = B_i^p(\xi) B_j^q(\eta) \quad (13)$$

The bivariate rational basis functions for a NURBS surface are then given as

$$N_{i,j}^{p,q}(\xi, \eta) = \frac{w_{i,j} B_i^p(\xi) B_j^q(\eta)}{\sum_{j=i=1}^n \sum_{j=1}^m w_{i,j} B_i^p(\xi) B_j^q(\eta)} \quad (14)$$

It is noted that the continuity and support of NURBS basis function are the same as for B-splines. Furthermore, when all the weights of control points have an equal positive constant value, the NURBS basis functions degenerate into the B-splines functions.

A NURBS surface is a bivariate piecewise rational function of the form:

$$\mathbf{S}(\xi, \eta) = \sum_{i=1}^n \sum_{j=1}^m N_{i,j}^{p,q}(\xi, \eta) \mathbf{P}_{i,j} \quad (15)$$

where  $\mathbf{P}_{i,j}$  are the control points.

### 3 IGA-MTOP-MMV design framework

#### 3.1 IGA-MTOP scheme

The classic ersatz material approach has been widely applied in many TO frameworks with immersed boundaries. This method is only applicable when the mesh is fine enough, because the mesh cannot recognise the structural features smaller than the mesh width. For example, in the top row of Fig. 4, three distinct structural patterns are identified the same in a coarse background mesh, because ersatz material property can be seen as the average of the element nodes and the differences of the three patterns are contained inside the elements. In such a circumstance, the background does not have enough resolution to distinguish the geometry features of three structural patterns. This could be a very noticeable problem, especially, the explicit description of MMV is totally decoupled from the background mesh, and is able to produce arbitrary small features. So, in MMV-TOP scheme, there is a demand for high resolution of the geometry [Liu, Zhu, Sun et al. (2018)].

When the background mesh is further refined, as shown in the bottom row of Fig. 4, the sub-elements (material elements) with the dashed line are capable of identifying the structural details. However, the fine mesh also means a large scale equilibrium equation, which is an obstacle of the computing efficiency. Thus, a multiresolution scheme is proposed to sense the material distribution with high-resolution without introducing DOFs to keep the computational cost at a relatively low level. Since the fine mesh is only used to identify the material distribution, and the analysis is still implemented on the coarse mesh, the multiresolution scheme does not enlarge the scale of the discretised equilibrium equation.

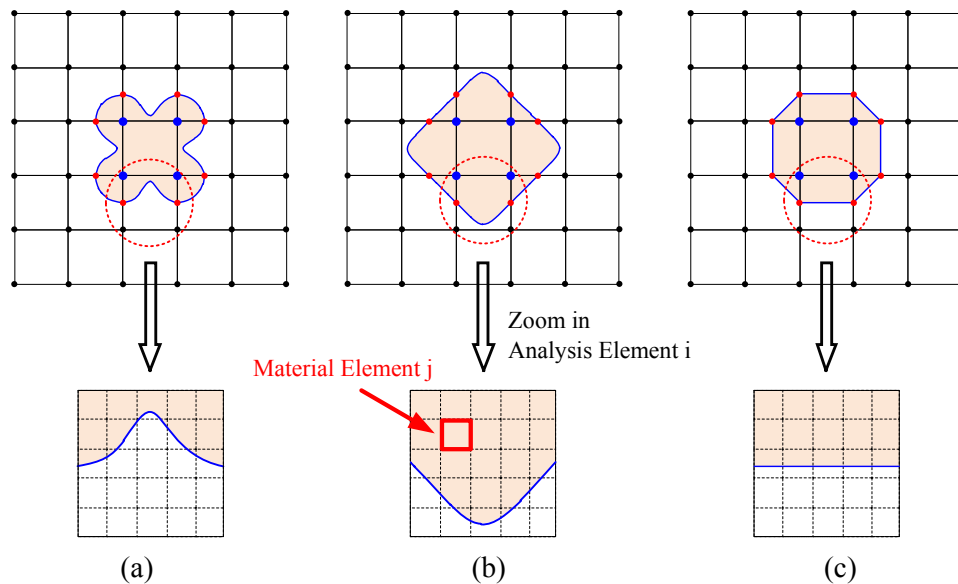


Figure 4: Identification of structural details in multiscale scheme

### 3.1.1 Space discretisation

The critical point of the multiresolution scheme is that one should make sure that the difference between the different high-resolution designs obtained using such schemes can be observed in the analysis results. To implement IGA-MTOP, a further variable parameter space is introduced to identify material distribution constructed with MMV. The same number of elements discretised for the analysis is again used in this space. To efficiently obtain high-resolution designs, each element is subdivided into  $ns \times ms$  subelements in the  $\xi$  and  $\eta$  directions, respectively. These subelements are called material elements hereafter in this article. An illustration of the analysis mesh and material mesh under the IGA-MTOP scheme is illustrated in Fig. 5. These functions can be easily obtained using the k-refinement strategy in the IGA, which has detailed in Hughes et al. [Hughes, Cottrell and Bazilevs (2005)].

### 3.1.2 Representation of material distribution

In order to represent the material distribution with refined material elements, the collocation scheme [Xie, Wang, Xu et al. (2018)] is utilised in this research. Specifically, Greville abscissae is adopted to identify the element density of the material elements with the ersatz material model. The  $j$ -th background element in the  $i$ -th analysis element is denoted as element  $(i, j)$ , as shown in Fig. 4(b). The Young's modulus and density of each material element can be calculated as

$$E^{i,j} = \frac{1}{n_{col}^{i,j}} \left( \sum_{icol=1}^{n_{col}^{i,j}} H^{reg} \left( T_{icol}^{i,j} \right) \right) E_0 \quad (16)$$

$$\rho^{i,j} = \frac{1}{n_{col}^{i,j}} \left( \sum_{icol=1}^{n_{col}^{i,j}} H \left( T_{icol}^{i,j} \right) \right) \quad (17)$$

in which,  $n_{col}^{i,j}$  and  $icol$  are the number and index of the collocation points,  $E_0$  is Young's modulus of the solid material,  $H \left( T_{icol}^{i,j} \right)$  is the regularized Heaviside value of  $icol$ -th collocation point,  $reg = 2$  is the regularised parameter.  $T_{icol}^{i,j}$  is TDF of the collocation point, which can be calculated with

It is approximated with the following formula:

$$H(T) = \begin{cases} \varepsilon, & T < -h \\ \frac{3(1-\varepsilon)}{4} \left( \frac{T}{h} - \left( \frac{T}{h} \right)^3 \right) + \frac{1+\varepsilon}{2}, & -h \leq T < h \\ 1, & T \geq h \end{cases} \quad (18)$$

In Eq. (18),  $\varepsilon$  is a small positive parameter, which ensures the nonsingularity of the global stiffness matrix. The level of regularization is controlled by the parameter  $h$ .

The Greville abscissae for each material elements can be constructed with the refined knot vectors. For a degree- $p$  NURBS with  $n$  control points and a length of  $n + p + 1$

knot vector  $\Xi = \{\xi_1, \xi_2, \dots, \xi_{n+p+1}\}$ , the Greville abscissae can be defined as

$$\zeta_i = \frac{1}{p}(\xi_{i+1} + \xi_{i+2} + \dots + \xi_{i+p}) \quad (19)$$

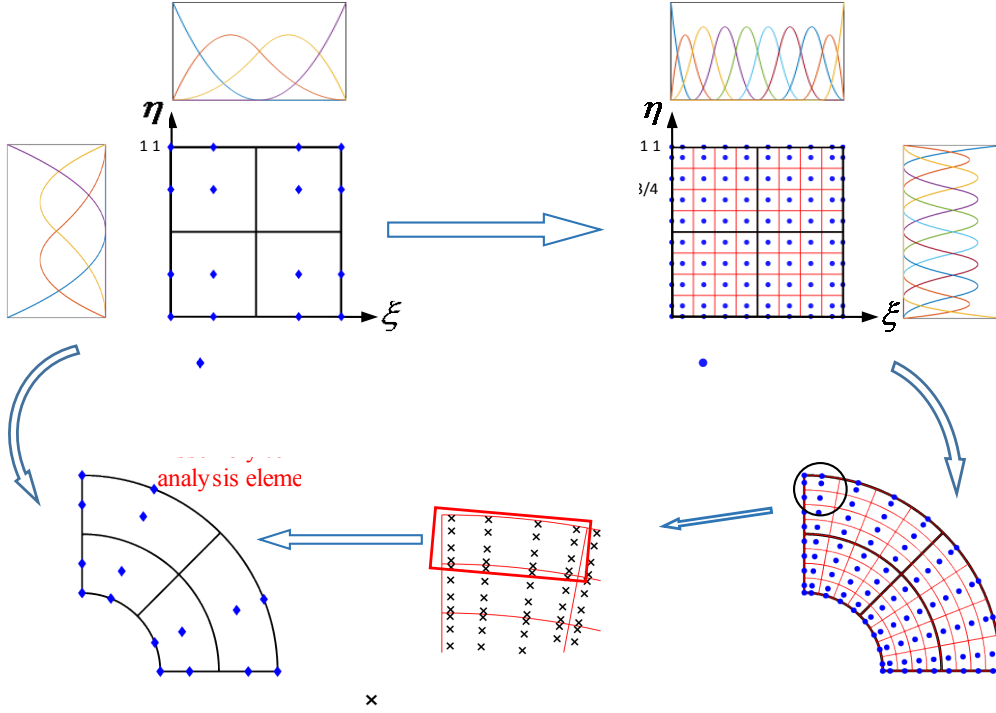


**Figure 5:** Distinct meshes for analysis and material in IGA-MTOP scheme

The stiffness contribution of each sub-element towards its analysis element can thus be calculated as

$$\begin{aligned} \mathbf{K}^{i,j} &= \int_{\Omega^{i,j}} \mathbf{B}_i^T(\xi^j, \eta^j) \mathbf{D}^{i,j} \mathbf{B}_i(\xi^j, \eta^j) |\mathbf{J}(\xi^j, \eta^j)| t d\Omega \\ &= \sum_J^{N_{gp}^{i,j}} w_J \mathbf{B}_i^T(\xi_J, \eta_J) \mathbf{D}^{i,j} \mathbf{B}_i(\xi_J, \eta_J) |\mathbf{J}(\xi_J, \eta_J)| t \end{aligned} \quad (20)$$

where  $\Omega^{i,j}$  is the  $j$ -th sub-domain of the  $i$ -th element, as shown in Fig. 5(d).  $J$  is the index of the Gaussian integration points,  $w_J$  is the weight.  $N_{gp}^{i,j}$  is the number of Gaussian points, which can be calculated as  $N_{gp}^{i,j} = (p+1)(q+1)$ .  $\mathbf{J}$  is the Jacobian determinant of the geometry mapping.  $\mathbf{B}_i$  is the element strain-displacement matrix composed of the basis derivatives of the  $i$ -th analysis element:

$$\mathbf{B} = \begin{bmatrix} \frac{\partial N_I}{\partial x} & 0 & \dots & \frac{\partial N_{I+(p+1)(q+1)-1}}{\partial x} & 0 \\ 0 & \frac{\partial N_I}{\partial y} & \dots & 0 & \frac{\partial N_{I+(p+1)(q+1)-1}}{\partial y} \\ \frac{\partial N_I}{\partial y} & \frac{\partial N_I}{\partial x} & \dots & \frac{\partial N_{I+(p+1)(q+1)-1}}{\partial y} & \frac{\partial N_{I+(p+1)(q+1)-1}}{\partial x} \end{bmatrix} \quad (21)$$

$I$  is the index of control points on the analysis mesh.  $\mathbf{D}^{i,j}$  is the constitutive matrix, which is defined as

$$\mathbf{D}^{i,j} = \frac{E^{i,j}}{1-\nu^2} \begin{bmatrix} 1 & \nu & 0 \\ \nu & 1 & 0 \\ 0 & 0 & \frac{1}{2}(1-\nu) \end{bmatrix} \quad (22)$$

The Young's modulus  $E^{i,j}$  is calculated from Eq. (16). Since the Gaussian quadrature of each material elements can be calculated and stored before the optimisation in the linear problems, the computation cost is considerably saved.

### 3.2 Sensitivity analysis

For simplicity, the compliance minimization under a volume constraint is solved in this article. The discrete equilibrium equation is reformulated as

$$\mathbf{K}\mathbf{U} = \sum_{i=1}^{nel} \mathbf{K}^i \mathbf{U} = \mathbf{F} \quad (23)$$

in which  $\mathbf{K}$ ,  $\mathbf{U}$  and  $\mathbf{F}$  are the global stiffness matrix, the displacement vector and external force vector, respectively.  $nel$  is the number of analysis elements,  $\mathbf{K}^i$  is the stiffness matrix of  $i$ -th analysis element, it equals to the sum of the stiffness of all material elements (shown in Figs. 5(d) and 5(c)):

$$\mathbf{K}^i = \sum_j^{ns \times ms} \mathbf{K}^{i,j} \quad (24)$$

The objective function for the compliance minimisation can be stated as

$$C = \sum_{i=1}^{nel} \mathbf{U}_i^T \mathbf{K}^i \mathbf{U}_i \quad (25)$$

Furthermore, the sensitivity of the structural compliance with respect to a design variable  $d$  can be expressed as

$$\frac{\partial C}{\partial d} = - \sum_{i=1}^{nel} \mathbf{U}_i^T \frac{\partial \mathbf{K}^i}{\partial d} \mathbf{U}_i \quad (26)$$

here  $d$  represent the coordinates of centres or the control radius. The derivation of  $i$ -th element stiffness matrix  $\mathbf{K}^i$  with respect to a design variable  $d$ , namely  $\partial \mathbf{K}^i / \partial d$  in Eq. (26), can be obtained according to Eqs. (16) and (24) as

$$\frac{\partial \mathbf{K}^i}{\partial d} = \frac{reg}{n_{col}^{i,j}} \sum_j^{ns \times ms} \left( \sum_{icol=1}^{n_{col}^{i,j}} H^{reg} \frac{\partial H(T_{icol}^{i,j})}{\partial d} \right) \quad (27)$$

The sensitivity of the volume can also be expressed:

$$\frac{\partial V}{\partial d} = - \sum_{i=1}^{nel} \sum_j^{ns \times ms} \sum_{icol=1}^{n_{col}^{i,j}} \frac{\partial H(T_{icol}^{i,j})}{\partial d} \quad (28)$$

#### 4 Numerical experiments

In this section, two numerical examples in 2D are provided to demonstrate the effectiveness and efficiency of the developed IGA-MTOP-MMV based design framework. First, the material description ability of the multiresolution scheme is validated, to find out whether detailed geometry features can be recognised by finer mesh. Then, a classic topology optimisation test example is employed to figure out the effectiveness of the proposed multiresolution isogeometric topology optimisation method based on moving morphable voids.

##### 4.1 Material field sensing test

The multiresolution scheme in this research is proposed to sense the distribution of material more accurately. Thus, the experiment in this section is arranged to test the representing ability of the material mesh with different resolution.

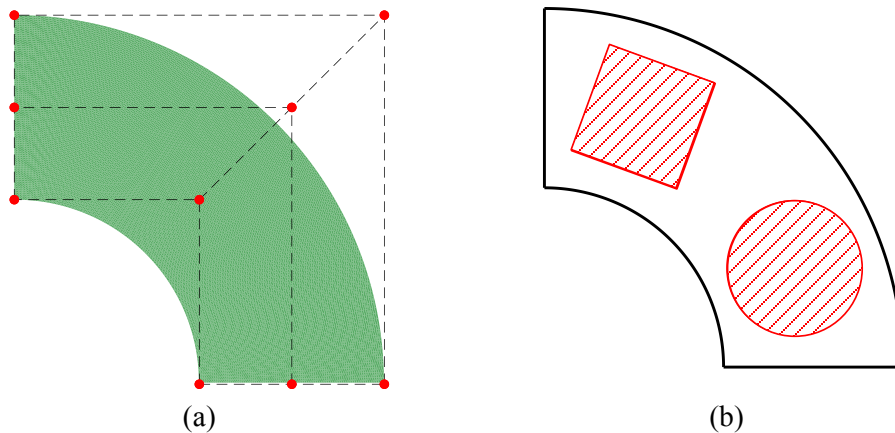


**Figure 6:** Material distribution of the design domain

As shown in Fig. 6(a), the design domain is quarter annulus that removes a rectangle and a circle, where the quarter is initially constructed by 9 control points (Fig. 6(a)). The positions of the rectangular and circular hole in the design domain are depicted in Fig. 6(b).

The goal of this example is to approximate the material field as close as possible with different material mesh. The collocation points are used to collocate the material field. The material distribution is visualised in Figs. 7(a)-7(d). The material interface is also

contoured to compare with the original material-remove area illustrated in Figs. 7(e)-7(h). As can be observed in (e), the  $32 \times 32$  mesh can generate a sufficiently good approximation of a circle area. However, it cannot approximate the rectangle well. When the resolution is increased, the approximation is also improved. The  $64 \times 64$  mesh coincides most of the boundary with the rectangle except for the sharp corner. As for  $128 \times 128$  and  $256 \times 256$ , they are capable of fitting the material field very well.

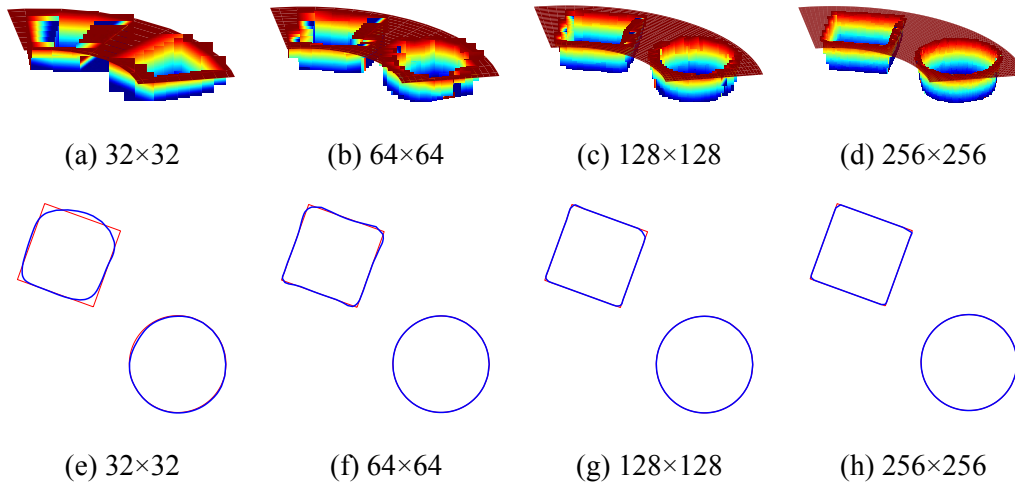


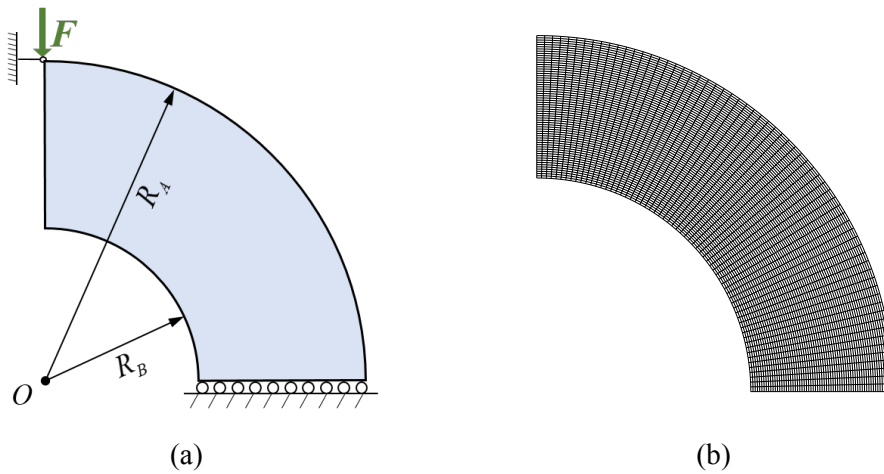
**Figure 7:** Approximation of the material field with different mesh

It can be observed that finer meshes can describe the material distribution more precisely, which verifies our expectation. In the next subsection, the refined material mesh is utilised in the optimisation with MMV.

#### 4.2 Quarter annulus

In this section, a quarter annulus with unit concentrated load and the boundary conditions are defined in Fig. 8(a), and two indices  $r$  and  $R$  are set as 5 and 10, respectively. All physical quantities are assumed to be dimensionless. The Young's moduli and Poisson's ratio for solid material are set to be 1 and 0.3, respectively. The thickness of the plate is also defined as 1. Its  $64 \times 64$  IGA mesh is shown in Fig. 8(b). The degrees are set to  $p = q = 3$ , and the number of Gaussian points for each material element is 16. The maximum material volume fraction is set as 40%.

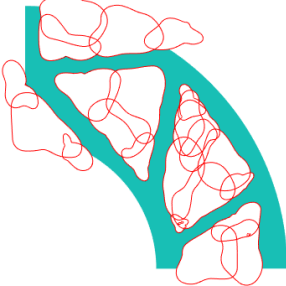
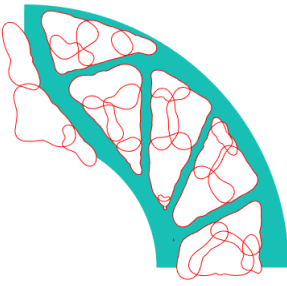
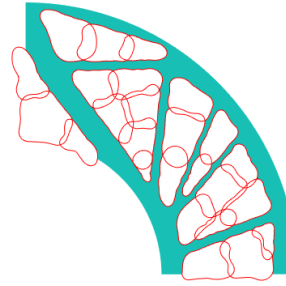
In order to show the influence of the resolution, the analysis mesh is refined 0, 1 and 2 times, resulting in the material mesh of  $64 \times 64$ ,  $128 \times 128$  and  $256 \times 256$ , respectively. For the convenience of observation, the PCBS are visualised with red curves. The initial layout of 25 voids is shown in Fig. 9(a). Each PCBS representing a void is constructed by 14 control points.



**Figure 8:** Quarter annulus: isogeometric analysis (IGA) elements  $64 \times 64$

The optimisation results are shown and compared in Tab. 1. All three design cases can converge to clear topologies, which demonstrates the effectiveness of the presented optimisation method based on MMV.

**Table 1:** The optimised design of quarter annulus in three cases

Material Mesh	$64 \times 64$	$128 \times 128$	$256 \times 256$
Optimised topology			
Obj	80.008	73.679	72.225
Time/Iteration	3.831 s	4.14 s	4.826 s
Num of iteration	293	257	200

Due to the limited resolution, the  $64 \times 64$  meshes generates a very coarse boundary and the largest compliance. The  $128 \times 128$  mesh can achieve visible improvement in the objective and the smoothness of the boundaries, which shows the effectiveness of the proposed scheme. The  $256 \times 256$  mesh further produces a structure with more details and the best

objectives among the three cases. All the cases share the same number of design variables and the same amount of analysis elements. No significant differences are found in the computation time of the MMA optimisation and the most time-consuming part of the IGA for the three cases. The difference lies in the calculation of TDF values and their derivatives of the collocation points. The  $128 \times 128$  mesh case consumes the largest elapsed time, which takes only 25.97% more than the  $64 \times 64$  mesh case. This example shows that the design can be significantly improved without refining the analysis mesh, just by using high-resolution material mesh.

We do not try higher resolution, because there is a bound for the improvement of resolution. Detailed derivation and discussion about this bound can be referred in Gupta et al. [Gupta, van der Veen, Aragón et al. (2017)].

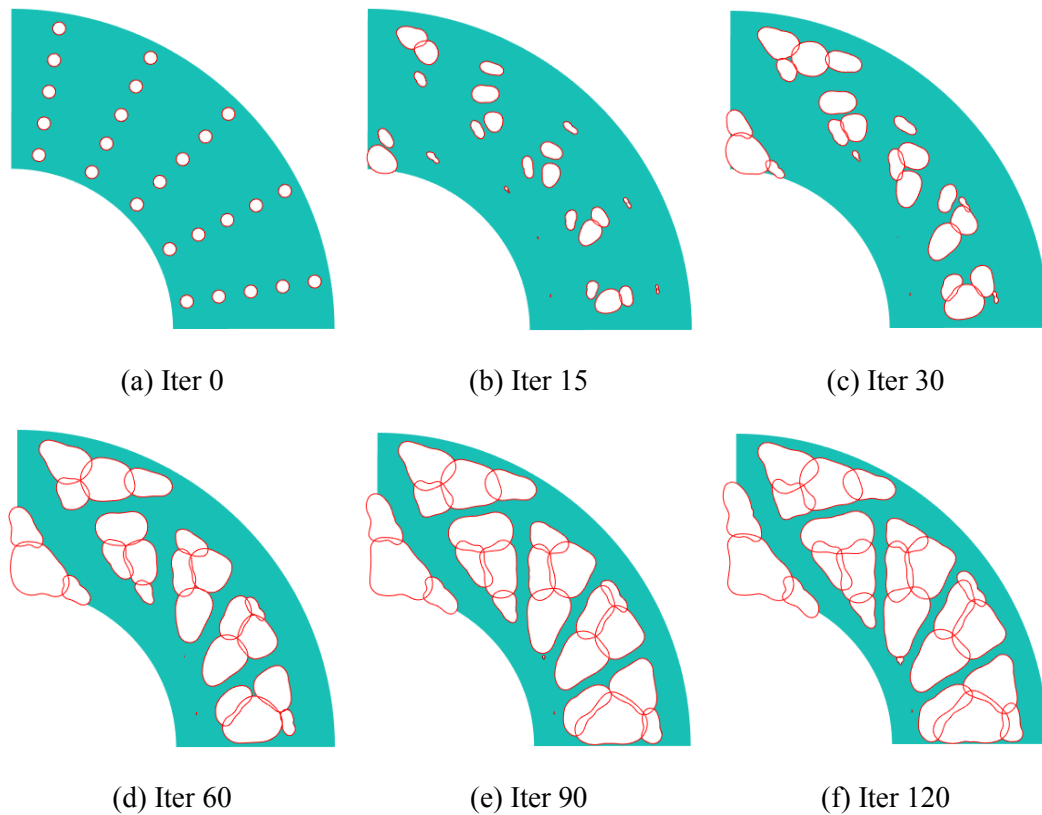


**Figure 9:** The intermediate structures during the optimisation

The iteration process of structural topology for  $128 \times 128$  mesh case is also visualised in Fig. 9 to give an insight into the optimisation process.

It is seen that, from the beginning to the 30th iteration, these voids expand a little to fulfil the volume constraints. The dominant behaviour of the voids is the movement of the centres: they move to find the advantageous location. From the Iter60, the layout of the voids does not change very much, and the structure evolves mainly through the change of boundaries.

Due to the explicit representation of the boundary, the void boundary can be easily generated, and can then be further merged and smoothed. By utilising the algorithm explained in Du et al. [Du, Yao, Zhao et al. (2019)], the CAD friendly boundary can be obtained. Take the optimised results of  $128 \times 128$  mesh case for example. Fig. 10(a) is the original optimised structure, Fig. 10(b) is the smoothed structure. Fig. 10(c) converts the intersected PCBS into continuous closed curves, which ensures every single hole in the structure can be represented by a single smoothed void.

## 5 Conclusions

In this work, an MMV-based approach for IGA-MTOP scheme has been proposed. Firstly, the IGA is successfully applied in the MMV based method, which is helpful to the integration of TO and CAD. Secondly, the multiresolution scheme brings benefits to the efficiency and optimality of the optimisation. In the MTOPT scheme, material mesh and the analysis mesh are separated. A fine material mesh is utilised to sense the material distribution more accurately, which is able to further release the advantages of the explicit nature of geometry description in the MMV-based solution framework. Since the analysis is still performed on the coarse mesh, high-resolution designs can be optimised with relatively low computational. The numerical examples also show that high resolution and more details can be obtained without introducing additional DOFs, which guarantees the efficiency of the scheme. The multiresolution IGA scheme is not only useful in MMV approach but also can be extended to MMC and level set methods which rely on the TDF value to describe the distribution of material.

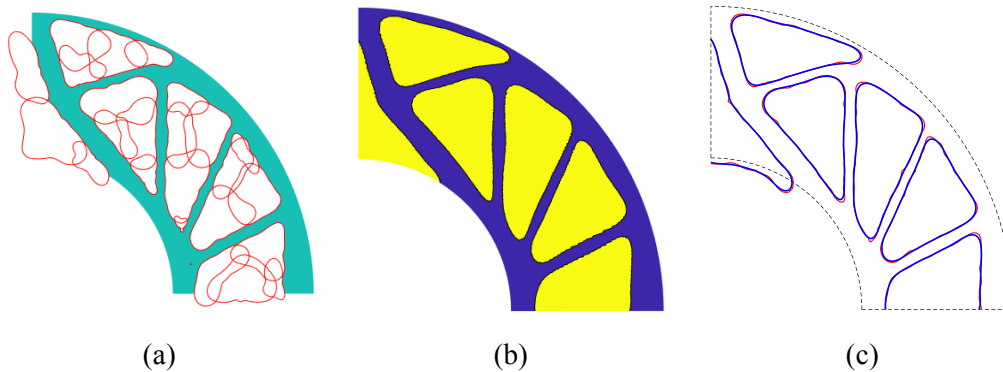


**Figure 10:** Illustration of boundary smoothing for  $128 \times 128$  case

Although the proposed scheme shows some merits, there are still many works to be done in the future. Firstly, the MMV method is still initial dependent, including the number, position and shape of the initial voids. A new MMV scheme which automatically introduces new holes to the design domain is expected. Secondly, it is also worthy to combine the adaptive scheme with MMV to solve the boundary sensitive problems, e.g., stress constrained problems. Moreover, the method should be tested more in the 3D scenario, which makes it more applicable in practical issues.

**Acknowledgement:** The authors would like to thank Professor Krister Svanberg at KTH in Stockholm for providing the implementation of MMA. This work was supported in part by National Natural Science Foundation of China under Grant Nos. 51675525 and 11725211.

**Conflict of Interest:** The authors declare that they have no conflicts of interest to report regarding the present study.

## References

- Allaire, G.; Jouve, F.; Toader, A. M.** (2004): Structural optimisation using sensitivity analysis and a level-set method. *Journal of Computational Physics*, vol. 194, no. 1, pp. 363-393.
- Bendsoe, M. P.; Kikuchi, N.** (1988): Generating optimal topologies in structural design using a homogenization method. *Computer Methods in Applied Mechanics & Engineering*, vol. 71, no. 2, pp. 197-224.
- Bendsøe, M. P.; Sigmund, O.** (2004): Topology optimisation: theory, methods, and applications: Springer Berlin Heidelberg, Berlin, Heidelberg.
- Bujny, M.; Aulig, N.; Olhofer, M.; Duddeck, F.** (2017): Evolutionary level set method for crashworthiness topology optimisation. *ECCOMAS Congress 2016*. pp. 309-322.
- Burla, R. K.; Kumar, A. V.** (2008): Implicit boundary method for analysis using uniform B-spline basis and structured grid. *International Journal for Numerical Methods in Engineering*, vol. 76, no. 13, pp. 1993-2028.
- Cottrell, J. A.; Hughes, T. J. R.; Bazilevs, Y.** (2009): Isogeometric analysis: toward integration of CAD and FEA: John Wiley & Sons.
- Dedè, L.; Borden, M. J.; Hughes, T. J. R.** (2012): Isogeometric analysis for topology optimisation with a phase field model. *Archives of Computational Methods in Engineering*, vol. 19, no. 3, pp. 427-465.
- Deng, J.; Chen, W.** (2016): Design for structural flexibility using connected morphable components based topology optimisation. *Science China Technological Sciences*, vol. 59, no. 6, pp. 839-851.
- Du, B.; Yao, W.; Zhao, Y.; Chen, X.** (2019): A moving morphable voids approach for topology optimisation with closed B-splines. *Journal of Mechanical Design, Transactions of the ASME*, vol. 141, no. 8, pp. 1-39.
- Du, X.; Zhu, F.** (2019): A novel principal components analysis (PCA) method for energy absorbing structural design enhanced by data mining. *Advances in Engineering Software*, vol. 127, pp. 17-27.
- Dunning, P. D.** (2017): Design parameterization for topology optimisation by intersection of an implicit function. *Computer Methods in Applied Mechanics & Engineering*, vol. 317, pp. 993-1011.
- Gao, J.; Gao, L.; Luo, Z.; Li, P.** (2019): Isogeometric topology optimisation for continuum structures using density distribution function. *International Journal for Numerical Methods in Engineering*, vol. 119, no. 10, pp. 991-1017.

- Ghasemi, H.; Park, H. S.; Rabczuk, T.** (2017): A level-set based IGA formulation for topology optimisation of flexoelectric materials. *Computer Methods in Applied Mechanics & Engineering*, vol. 313, pp. 239-258.
- Guest, J. K.; Prévost, J. H.; Belytschko, T.** (2004): Achieving minimum length scale in topology optimisation using nodal design variables and projection functions. *International Journal for Numerical Methods in Engineering*, vol. 61, no. 2, pp. 238-254.
- Guo, X.; Zhang, W.; Zhong, W.** (2014): Doing topology optimisation explicitly and geometrically-a new moving morphable components based framework. *Journal of Applied Mechanics*, vol. 81, no. 8, pp. 81009.
- Gupta, D. K.; van der Veen, G. J.; Aragón, A. M.; Langelaar, M.; van Keulen, F.** (2017): Bounds for decoupled design and analysis discretisations in topology optimisation. *International Journal for Numerical Methods in Engineering*, vol. 111, no. 1, pp. 88-100.
- Hassani, B.; Khanzadi, M.; Tavakkoli, S. M.** (2012): An isogeometrical approach to structural topology optimisation by optimality criteria. *Structural and Multidisciplinary Optimisation*, vol. 45, no. 2, pp. 223-233.
- He, Q.; Kang, Z.; Wang, Y.** (2014): A topology optimisation method for geometrically nonlinear structures with meshless analysis and independent density field interpolation. *Computational Mechanics*, vol. 54, no. 3, pp. 629-644.
- Hou, W.; Gai, Y.; Zhu, X.; Wang, X.; Zhao, C. et al.** (2017): Explicit isogeometric topology optimisation using moving morphable components. *Computer Methods in Applied Mechanics & Engineering*, vol. 326, pp. 694-712.
- Huang, X.; Xie, Y. M.** (2007): Convergent and mesh-independent solutions for the bi-directional evolutionary structural optimisation method. *Finite Elements in Analysis and Design*, vol. 43, no. 14, pp. 1039-1049.
- Hughes, T. J. R.; Cottrell, J. A.; Bazilevs, Y.** (2005): Isogeometric analysis: CAD, finite elements, NURBS, exact geometry and mesh refinement. *Computer Methods in Applied Mechanics & Engineering*, vol. 194, no. 39-41, pp. 4135-4195.
- Jahangiry, H. A.; Tavakkoli, S. M.** (2017): An isogeometrical approach to structural level set topology optimisation. *Computer Methods in Applied Mechanics & Engineering*, vol. 319, pp. 240-257.
- Kumar, A. V.; Parthasarathy, A.** (2011): Topology optimisation using B-spline finite elements. *Structural and Multidisciplinary Optimisation*, vol. 44, no. 4, pp. 471-481.
- Li, H.; Li, P.; Gao, L.; Zhang, L.; Wu, T.** (2015): A level set method for topological shape optimisation of 3D structures with extrusion constraints. *Computer Methods in Applied Mechanics & Engineering*, vol. 283, pp. 615-635.
- Lieu, Q. X.; Lee, J.** (2017a): A multi-resolution approach for multi-material topology optimisation based on isogeometric analysis. *Computer Methods in Applied Mechanics & Engineering*, vol. 323, pp. 272-302.
- Lieu, Q. X.; Lee, J.** (2017b): Multiresolution topology optimisation using isogeometric analysis. *International Journal for Numerical Methods in Engineering*, vol. 112, no. 13, pp. 2025-2047.

- Liu, C.; Du, Z.; Zhang, W.; Zhu, Y.; Guo, X.** (2017): Additive manufacturing-oriented design of graded lattice structures through explicit topology optimisation. *Journal of Applied Mechanics, Transactions ASME*, vol. 84, no. 8, 081008.
- Liu, Y.; Li, Z.; Wei, P.; Wang, W.** (2018): Parameterised level-set based topology optimisation method considering symmetry and pattern repetition constraints. *Computer Methods in Applied Mechanics & Engineering*, vol. 340, pp. 1079-1101.
- Liu, H.; Yang, D.; Hao, P.; Zhu, X.** (2018): Isogeometric analysis based topology optimisation design with global stress constraint. *Computer Methods in Applied Mechanics & Engineering*, vol. 342, pp. 625-652.
- Liu, C.; Zhu, Y.; Sun, Z.; Li, D.; Du, Z. et al.** (2018): An efficient moving morphable component (MMC)-based approach for multi-resolution topology optimisation. *Structural and Multidisciplinary Optimisation*, vol. 58, no. 6, pp. 2455-2479.
- Van Miegroet, L.; Duysinx, P.** (2007): Stress concentration minimization of 2D filets using X-FEM and level set description. *Structural and Multidisciplinary Optimisation*, vol. 33, no. 4-5, pp. 425-438.
- Nguyen, T. H.; Paulino, G. H.; Song, J.; Le, C. H.** (2010): A computational paradigm for multiresolution topology optimisation (MTOPT). *Structural and Multidisciplinary Optimisation*, vol. 41, no. 4, pp. 525-539.
- Norato, J. A.; Bell, B. K.; Tortorelli, D. A.** (2015): A geometry projection method for continuum-based topology optimisation with discrete elements. *Computer Methods in Applied Mechanics & Engineering*, vol. 293, pp. 306-327.
- Piegl, L.; Tiller, W.** (2013): *The NURBS Book*. Springer Berlin Heidelberg, Berlin, Heidelberg.
- Qian, X.** (2013): Topology optimisation in B-spline space. *Computer Methods in Applied Mechanics & Engineering*, vol. 265, pp. 15-35.
- Svanberg, K.** (1987): The method of moving asymptotes-a new method for structural optimisation. *International Journal for Numerical Methods in Engineering*, vol. 24, no. 2, pp. 359-373.
- Wang, Z. P.; Abdalla, M.; Turteltaub, S.** (2017): Normalization approaches for the descent search direction in isogeometric shape optimisation. *CAD Computer Aided Design*, vol. 82, pp. 68-78.
- Wang, Y.; Arabnejad, S.; Tanzer, M.; Pasini, D.** (2018): Hip implant design with three-dimensional porous architecture of optimized graded density. *Journal of Mechanical Design*, vol. 140, no. 11, pp. 111406.
- Wang, Y.; Benson, D. J.** (2016a): Geometrically constrained isogeometric parameterised level-set based topology optimisation via trimmed elements. *Frontiers of Mechanical Engineering*, vol. 11, no. 4, pp. 328-343.
- Wang, Y.; Benson, D. J.** (2016b): Isogeometric analysis for parameterised LSM-based structural topology optimisation. *Computational Mechanics*, vol. 57, no. 1, pp. 19-35.
- Wang, Y.; Kang, Z.; He, Q.** (2013): An adaptive refinement approach for topology optimisation based on separated density field description. *Computers & Structures*, vol. 117, no. Supplement C, pp. 10-22.

- Wang, Y.; Liao, Z.; Ye, M.; Zhang, Y.; Li, W. et al.** (2020): An efficient isogeometric topology optimisation using multilevel mesh, MGCG and local-update strategy. *Advances in Engineering Software*, vol. 139, pp. 102733.
- Wang, X.; Long, K.; Hoang, V. N.; Hu, P.** (2018): An explicit optimisation model for integrated layout design of planar multi-component systems using moving morphable bars. *Computer Methods in Applied Mechanics & Engineering*, vol. 342, pp. 46-70.
- Wang, Z. P.; Turteltaub, S.; Abdalla, M.** (2017): Shape optimisation and optimal control for transient heat conduction problems using an isogeometric approach. *Computers & Structures*, vol. 185, pp. 59-74.
- Wang, M. Y.; Wang, X.; Guo, D.** (2003): A level set method for structural topology optimisation. *Computer Methods in Applied Mechanics & Engineering*, vol. 192, no. 1-2, pp. 227-246.
- Wang, Y.; Wang, Z.; Xia, Z.; Poh, L. H.** (2018): Structural design optimisation using isogeometric analysis: a comprehensive review. *Computer Modeling in Engineering & Sciences*, vol. 117, no. 3, pp. 455-507.
- Wei, P.; Li, Z.; Li, X.; Wang, M. Y.** (2018): An 88-line MATLAB code for the parameterised level set method based topology optimisation using radial basis functions. *Structural and Multidisciplinary Optimisation*, vol. 58, no. 2, pp. 831-849.
- Wei, P.; Ma, H.; Wang, M. Y.** (2014): The stiffness spreading method for layout optimisation of truss structures. *Structural and Multidisciplinary Optimisation*, vol. 49, no. 4, pp. 667-682.
- Wei, P.; Wang, M. Y.; Xing, X.** (2010): A study on X-FEM in continuum structural optimisation using a level set model. *Computer-Aided Design*, vol. 42, no. 8, pp. 708-719.
- Xia, Z.; Wang, Y.; Wang, Q.; Mei, C.** (2017): GPU parallel strategy for parameterised LSM-based topology optimisation using isogeometric analysis. *Structural and Multidisciplinary Optimisation*, vol. 56, no. 2, pp. 413-434.
- Xie, X.; Wang, S.; Xu, M.; Wang, Y.** (2018): A new isogeometric topology optimisation using moving morphable components based on R-functions and collocation schemes. *Computer Methods in Applied Mechanics & Engineering*, vol. 339, pp. 61-90.
- Xu, M.; Wang, S.; Xie, X.** (2019): Level set-based isogeometric topology optimisation for maximizing fundamental eigenfrequency. *Frontiers of Mechanical Engineering*, vol. 14, no. 2, pp. 222-234.
- Xue, R.; Liu, C.; Zhang, W.; Zhu, Y.; Tang, S. et al.** (2019): Explicit structural topology optimisation under finite deformation via Moving Morphable Void (MMV) approach. *Computer Methods in Applied Mechanics & Engineering*, vol. 344, pp. 798-818.
- Yoely, Y. M.; Amir, O.; Hanniel, I.** (2018): Topology and shape optimisation with explicit geometric constraints using a spline-based representation and a fixed grid. *Procedia Manufacturing*, vol. 21, pp. 189-196.
- Zhang, W.; Li, D.; Zhang, J.; Xu, G.** (2016): Minimum length scale control in structural topology optimisation based on the Moving Morphable Components (MMC) approach. *Computer Methods in Applied Mechanics & Engineering*, vol. 311, no. August, pp. 327-355.

**Zhang, W.; Li, D.; Zhou, J.; Du, Z.; Li, B. et al.** (2018): A moving morphable void (MMV)-based explicit approach for topology optimisation considering stress constraints. *Computer Methods in Applied Mechanics & Engineering*, vol. 334, pp. 381-413.

**Zhang, S.; Norato, J. A.; Gain, A. L.; Lyu, N.** (2016): A geometry projection method for the topology optimisation of plate structures. *Structural and Multidisciplinary Optimisation*, vol. 54, no. 5, pp. 1-18.

**Zhang, W.; Yang, W.; Zhou, J.; Li, D.; Guo, X.** (2017): Structural topology optimisation through explicit boundary evolution. *Journal of Applied Mechanics, Transactions ASME*, vol. 84, no. 1.

**Zhang, W.; Zhang, J.; Guo, X.** (2016): Lagrangian description based topology optimisation-a revival of shape optimisation. *Journal of Applied Mechanics*, vol. 83, no. 4, pp. 41010.

**Zhang, W.; Zhao, L.; Gao, T.; Cai, S.** (2017): Topology optimisation with closed B-splines and Boolean operations. *Computer Methods in Applied Mechanics & Engineering*, vol. 315, pp. 652-670.

**Zhang, W.; Zhou, Y.; Zhu, J.** (2017): A comprehensive study of feature definitions with solids and voids for topology optimisation. *Computer Methods in Applied Mechanics & Engineering*, vol. 325, pp. 289-313.

**Zhou, Y.; Zhang, W.; Zhu, J.** (2019): Concurrent shape and topology optimisation involving design-dependent pressure loads using implicit B-spline curves. *International Journal for Numerical Methods in Engineering*, vol. 118, no. 9, pp. 495-518.